Fast-Tracking Transition State Localization via Reaction Directional Analysis

Peipei Zhang[a], Chenxi Guo[*b] and P. Hu[*a,c,d]

[a] *Key Laboratory for Advanced Materials, Research Institute of Industrial Catalysis and Centre for Computational Chemistry, East China University of Science and Technology, Shanghai, 200237, China*
[b] *Industrial AI Technic Center, SUPCON Technology Co., Ltd., Hangzhou, 310053, China*
[c] *School of Physical Science and Technology, ShanghaiTech University, Shanghai 201210, China*
[d] *School of Chemistry and Chemical Engineering, The Queen's University of Belfast, Belfast BT9 5AG, United Kingdom*

* Corresponding authors. Emails:
guochenxi@supcon.com
hupj@shanghaitech.edu.cn

ABSTRACT:

Transition state localization is critical for elucidating chemical reaction mechanisms but remains one of the most computationally demanding challenges in theoretical chemistry. Here, we introduce a novel method, Reaction Directional Analysis-Dimer (RDA-D), which integrates reaction directional analysis (RDA) with the dimer method to achieve efficient and reliable transition state searching. Reaction directional analysis generates high-quality quasi-transition-state structures directly from only the initial and final state geometries, combining dynamic interpolation, structure optimization, and directional analysis. These quasi-transition-state structures then serve as starting points for refinement via the dimer method. Benchmark tests on a diverse set of gas-phase and catalytic reactions on surfaces demonstrate that RDA-D is, on average, 5.70 times faster than the Nudged Elastic Band (NEB) method in CPU time and reduces the number of gradient evaluations by a factor of 4.67. Moreover, reaction directional analysis eliminates the need for predefined reaction coordinates or chemically intuitive initial guesses, providing a robust, scalable, and automation-friendly framework for transition state localization.

1. INTRODUCTION

Transition state (TS) identification is a cornerstone of computational chemistry, critical for calculating energy barriers, constructing potential energy surfaces (PES), and understanding reaction mechanisms and reaction kinetics.[1-6] Despite its importance, two major challenges persist in TS calculations: (i) the computational cost is significantly higher than those of locating reaction initial and final states; and (ii) it often relies on expert knowledge and manual intervention, especially for complex systems with high-dimensional PES landscapes.

Traditional methods for TS searches, such as the Nudged Elastic Band (NEB),[7-10] the string method[11, 12] and related approaches,[13, 14] typically begin by a construction of specific reaction pathway between initial state (IS) and final state (FS). The TS is then identified by optimizing this path. Although these path-based strategies provide reliable and stable TS identification, their computational efficiency is often limited by the optimizations of multiple images, which traverse the potential energy surface. For complex reactions, these limitations manifest as high computational costs and difficulties on the convergence for the rigorous TS. To overcome these limitations, various improvements have been developed.[3, 15-17] For example, the climbing image nudged elastic band (CI-NEB) method combined with energy-weighted (EW) springs, referred to as EW-CI-NEB, introduces energy-weighted springs between the interpolated images, resulting in a denser distribution of images in the transition state region along the reaction coordinate. This modification increases accuracy in the vicinity of the saddle point.[18] Furthermore, the EW-CI-NEB approach was integrated with an eigenvector-following (EF) method: After EW-CI-NEB brings the images close to the transition state along the defined reaction coordinate, the EF method is automatically invoked using the climbing image and its tangent as the initial guess, and precisely optimize the geometry to the true transition state.[19] Despite these targeted improvements, current approaches seldom resolve both computational efficiency and stability simultaneously, and the associated computational costs remain a significant challenge. It is clear that, while these advances have enhanced either the efficiency or accuracy of TS searches, persistent issues regarding computational expense and robustness have yet to be fully solved.

In contrast to path-based methods, another major class of transition state (TS) search algorithms relies on initializing the process with a guessed TS structure. Techniques such as the dimer method,[20] constrained optimization methods,[21-24] constrained Broyden dimer (CBD),[25-28] and rational function optimization (RFO)[29-31] all leverage initial guesses and local potential energy surface information to expedite optimization. Compared to path-based strategies, these approaches can significantly reduce computational costs and improve efficiency. However, their performance is heavily dependent on the quality of the provided initial guesses. Inaccurate or poorly chosen initial structures may result in poor convergence or unreliable outcomes. This dependence limits the applicability of these methods, especially for unfamiliar or complex reactions where suitable initial guesses are difficult to obtain.

Given these observations, the development of robust and automated strategies for

generating high-quality initial guesses is becoming increasingly important. The Growing String Method (GSM)[32, 33] constructs initial guesses for TS searches by growing reaction paths from both the IS and FS and merging them in the middle, thereby producing a pathway that is often more physically realistic. Nevertheless, GSM typically requires multiple optimizations of the path nodes, leading to higher computational cost, and it is susceptible to being trapped in local minima, which may hinder convergence in complex systems. Recently, Sun et al.[34] proposed applying the fast marching tree (FMT) path planning algorithm to free energy landscapes (FEL), which can automatically identify a minimum-energy path as an initial guess when a FEL is available. However, the effectiveness of this approach is contingent upon the quality and dimensionality of the FEL, and parameter selection still involves a degree of empirical tuning. Achieving fully automatic optimization and adapting these methods to diverse chemical systems remain unresolved challenges. Therefore, the development of efficient, automated, and reliable protocols for generating initial guesses is of critical importance for advancing TS search methodologies, particularly for complex or high-dimensional systems.

In this work, we propose a novel strategy, termed reaction directional analysis (RDA), for efficient and automated transition state (TS) localization. RDA generates a high-quality quasi-transition-state structure directly from the initial state (IS) and final state (FS) geometries, which then serves as the starting point for refinement via the dimer method. The combined approach, referred to as RDA-D, ensures reliable and accurate TS optimization. The main advantage of RDA-D lies in its ability to eliminate reliance on chemical intuition or predefined reaction coordinates for initial guesses. By integrating dynamic interpolation, structural screening, and reaction directional analysis, RDA greatly accelerates the identification of suitable quasi-TS candidates, making the entire TS search process highly amenable to automation. When benchmarked against the conventional Nudged Elastic Band (NEB) method using identical IS and FS as inputs, the RDA-D workflow achieves substantial reductions in computational cost while maintaining quantitative accuracy. For 24 gas-phase reactions from Baker's benchmark dataset,[35] RDA-D is on average approximately 6.42 times faster than NEB in terms of CPU time, and requires about 4.25 times fewer gradient calculations. For a set of 8 catalytic reactions occurring on Pt(111) and Pt(211), RDA-D achieves a speedup of about 4.64 times in CPU time and 6.05 times fewer gradient calculations compared to NEB. In the following sections, the detailed workflow of the RDA methodology, its integration with the dimer approach, and its performance across benchmark reactions are presented.

2. METHOD

2.1 Transition state definition

During a chemical reaction, the initial state (IS) may evolve into the final state (FS) through multiple possible pathways on the potential energy surface (PES), as illustrated in Figure 1. Among these, the minimum energy path (MEP) connects IS and FS through the lowest possible energy barrier, and the highest point along this path corresponds to

the transition state (TS).

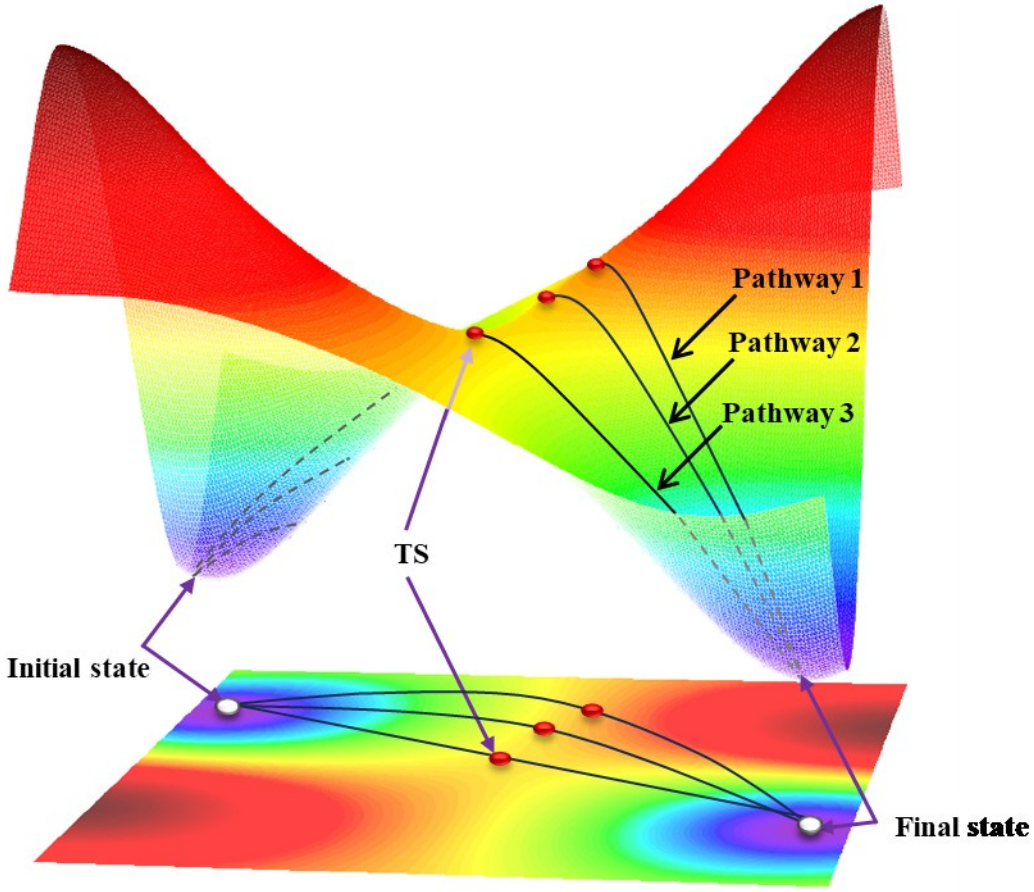

Figure 1. Schematic representation of various possible pathways linking the initial and final states on a potential energy surface (PES). The pathways are shown as black lines, while the corresponding energy maximum (EM) points along each pathway are indicated by red dots. Among these, pathway 3 possesses the EM point with the lowest energy, which corresponds to the exact transition state (TS) connecting the initial and final states.

In the schematic representation, pathway 3 represents the MEP, with its highest point corresponding to the transition state. The primary goal of our work is to efficiently and accurately locate the TS along this path.

2.2 General workflow for RDA-D

In this work, we introduce a methodology termed RDA-D, which integrates reaction directional analysis with dimer-based transition state refinement. RDA-D is briefly outlined below and details are provided in the following sections. Figure 2 illustrates the general workflow.

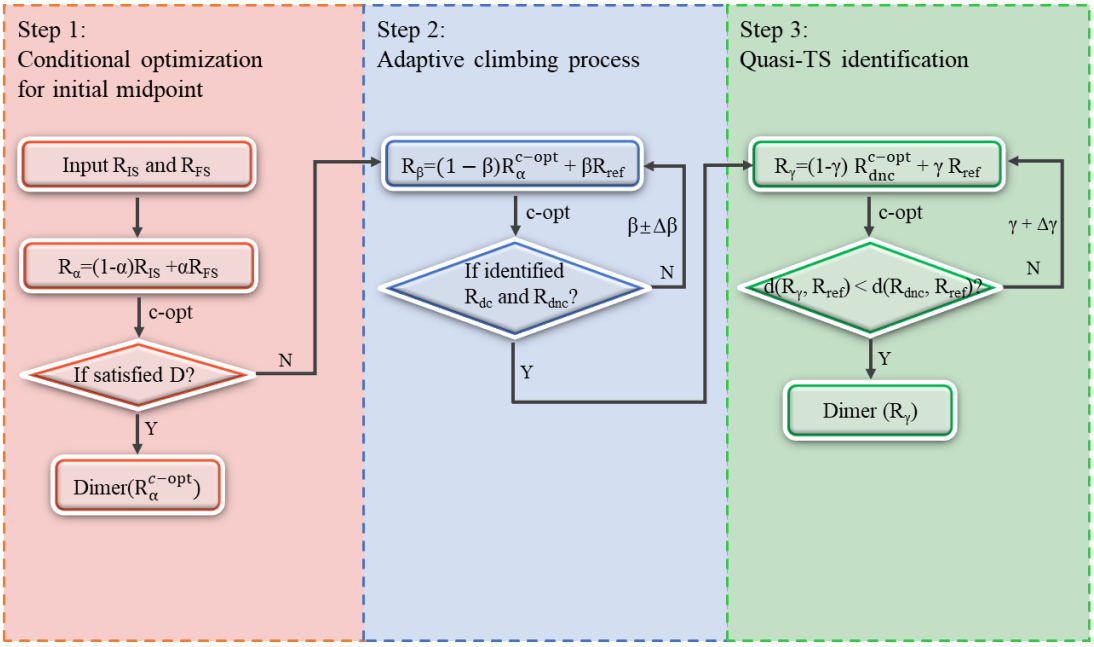

Figure 2. Workflow of the reaction directional analysis combined with the dimer (RDA-D) method.

In general, the RDA-D procedure begins by constructing the midpoint structure between the IS and FS, followed by a conditional optimization (c-opt, see details in Section 2.3.1). If the conditionally optimized structure satisfies the preliminary criteria for a TS candidate (Section 2.3.4), the dimer search is performed directly. Otherwise, the workflow proceeds to an adaptive climbing process, in which new candidates are generated by interpolating between the optimized structure and a reference state (Section 2.4.1; reference state selection in Section 2.3.3). Directionality analysis is then applied to the iteratively optimized candidates until two structures with opposite directionality are identified, thereby bracketing the TS region (Section 2.4.2). Additional candidates are subsequently generated between one of the identified bracketing structures (Section 2.4.2) and the reference structure. The candidate closest to the bracketing structure and geometrically nearer to the transition state region is designated as the quasi-transition state. The quasi-transition state serves as the initial guess for the dimer method, which then converges to the precise transition state (Section 2.4.3).

2.3 Reaction Directional Analysis

Reaction directional analysis (RDA) combines dynamic interpolation, structural optimization, directional analysis, and candidate structure screening to efficiently and reliably identify quasi-transition state (quasi-TS), while minimizing computational cost and avoiding artifacts associated with optimization convergence. This automated workflow systematically explores reaction pathways, enabling robust localization of TSs.

2.3.1 Convergence Criteria for Conditional Optimization (c-opt)

In this work, we introduce a specialized optimization procedure, namely conditional

optimization (c-opt), in which convergence is determined by the energy difference (ΔE) between consecutive optimization steps rather than by conventional force threshold:

$$\Delta E = E_n - E_{n-1} \quad (1)$$

When ΔE approaches zero, it indicates that structural changes are minimal and the optimization process is close to convergence. In the context of interpolated images along a reaction pathway, this criterion prevents over-optimization of intermediate structures towards the initial or final states, ensuring that they remain close to the intended reaction pathway rather than fully relaxing into the minima.

To balance accuracy and efficiency, a dual-threshold conditional optimization (c-opt) scheme was used. Given that interpolated structures generated in the initial stage may be far from the true reaction pathway, a stringent convergence threshold $\Delta E < 0.01$ eV was applied for the c-opt procedures in step 1. Once generated structures were close to the reaction pathway, namely in step 2, a more relaxed threshold of $\Delta E < 0.05$ eV was used. This dual-threshold strategy enables efficient optimization toward the saddle region while minimizing computational cost and is applied only in Steps 1 and 2 of the RDA-D.

2.3.2 Determination of Labels in RDA

During the RDA calculations, a variety of intermediate structures are generated, and a systematic nomenclature is introduced to denote them. The notation R is used to represent a molecular structure, with superscripts and subscripts indicating specific characteristics. Superscripts correspond to the step of the conditional optimization process: a numeric superscript denotes the structure at a particular optimization step (e.g., R^n for the structure at the n^{th} step), while $R^{c\text{-}opt}$ refers to the structure obtained after completion of conditional optimization.

Subscripts indicate particular states or roles of the structure: R_{IS} and R_{FS} denote the initial and final states, respectively; R_{ref} represents the reference structure used during the interpolation process, which may be either the R_{IS} or R_{FS}. The specific definition and selection of the reference structure are described in Section 2.3.3.

Interpolation is employed in Step 1-3 of the workflow, with the interpolation ratios denoted by the Greek letters α, β, and γ in each respective step. For example, in Step 1, the interpolated structure

$$R_\alpha = (1-\alpha)R_{IS} + \alpha R_{FS} \quad (2)$$

represents a combination of the initial and final states, where the R_{IS} contributes a fraction of $1-\alpha$, and the R_{FS} contributes a fraction of α. In general, linear interpolation[36] is applied. However, in rare cases where the interpolated structures display significant distortions already in the early stages of conditional optimization, the image-dependent pair potential (IDPP) interpolation method[37] is used as a complementary approach to generate smoother initial pathways.

2.3.3 Directional Analysis

The Euclidean distance (d) is employed to quantitatively measure the geometric difference between two structures. For any two structures R_1 and R_2, the Euclidean distance d is defined as follows:

$$d(\mathrm{R}_1, \mathrm{R}_2) = \sqrt{\sum_{x=1}^{N} [(\mathrm{R}_1(x) - \mathrm{R}_2(x)]^2} \quad (3)$$

where $R_1(x)$ and $R_2(x)$ denote the coordinates of atom x in R_1 and R_2, respectively, and N is the total number of atoms. This metric is employed throughout the workflow to monitor the structural evolution during optimization and to evaluate the proximity of a given structure to the IS, FS, or the TS.

The directionality of structural evolution is analyzed by evaluating the Euclidean distance between each intermediate structure and the IS or FS. Specifically, changes in $d(\mathrm{R}, \mathrm{R_{IS}})$ and $d(\mathrm{R}, \mathrm{R_{FS}})$ are tracked during the conditional optimization process. A decrease in $d(\mathrm{R}, \mathrm{R_{IS}})$ indicates movement towards the initial state, whereas a decrease in $d(\mathrm{R}, \mathrm{R_{FS}})$ suggests approach to the final state. The directionality is formally determined by the sign and magnitude of the Euclidean distance differences (Δd), enabling the identification of the reaction coordinate's progression.

$$\Delta \mathrm{d_{IS}}(\mathrm{R^{c-opt}}) = \mathrm{d}\,(\mathrm{R^{c-opt}}, \mathrm{R_{IS}}) - \mathrm{d}\,(\mathrm{R^1}, \mathrm{R_{IS}}) \quad (4)$$

$$\Delta \mathrm{d_{FS}}(\mathrm{R^{c-opt}}) = \mathrm{d}\,(\mathrm{R^{c-opt}}, \mathrm{R_{FS}}) - \mathrm{d}\,(\mathrm{R^1}, \mathrm{R_{FS}}) \quad (5)$$

where, $R^{c\text{-}opt}$ denotes the structure that has converged according to the conditional optimization criterion, R^1 corresponds to the structure optimized in the first step, i.e., the initial structure. R_{IS} and R_{FS} represent the initial state (IS) or final state (FS) structure, respectively. The Euclidean distance differences Δd provides a robust metric for evaluating structural positions relative to reaction coordinates and potential TS proximity. A larger $|\Delta d|$ indicates significant atomic positional changes during optimization process, while a smaller $|\Delta d|$ implies greater similarity between $\mathrm{R^{c-opt}}$ and $\mathrm{R^1}$.

The directionality $\sigma(R^{c\text{-}opt})$ is defined as:

$$\sigma(\mathrm{R^{c-opt}}) = \begin{cases} \text{IS} & \Delta d_{IS} < 0, \Delta d_{FS} > 0 \\ \text{FS} & \Delta d_{IS} > 0, \Delta d_{FS} < 0 \\ \text{Nondirectional} & \Delta d_{IS} \cdot \Delta d_{FS} > 0 \end{cases} \quad (6)$$

It should be noted that, in practical applications, there are cases where both directionality indicators are simultaneously positive, as illustrated in Figure 3b. In such scenarios, the interpretation and handling of directionality are further elaborated and discussed in detail in Section 2.3.4.

Furthermore, when performing interpolation between the conditionally optimized structure and the reference structure, the choice of the R_{ref} is determined by the optimization direction: if the directionality indicates movement toward IS, then FS is selected as the new R_{ref}, and vice versa.

2.3.4 Determination Criteria

To address the issue of both directionality indicators being simultaneously positive (i.e., the structure fails to converge towards either the initial or final state, see Section 2.3.3) and to further improve computational efficiency, we establish a set of quantitative criteria, collectively referred to as the D criteria. These criteria are used to assess whether an intermediate structure located sufficiently close to the TS region.

A schematic illustration of possible scenarios during conditional optimization is shown in Figure 3a. If the conditionally optimized structure satisfies any of the criteria below, it is considered to be near the TS. In such instances, the dimer method is applied directly to this structure without the need for the additional climbing procedure (step 2, see details in 2.4.2), thereby streamlining the overall TS search process.

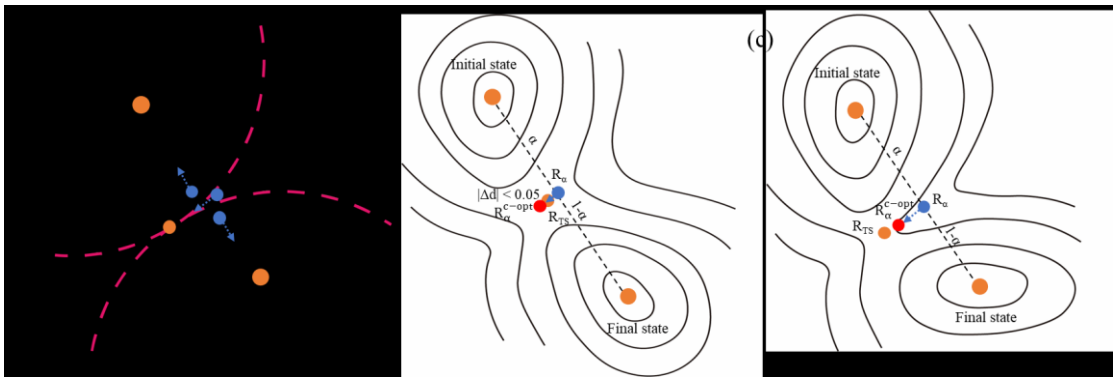

Figure 3. Representative scenarios of conditional optimization during reaction directional analysis (RDA): (a) Schematic illustration of optimization directions at different positions on the PES. (b) Case where both $|\Delta d_{IS}| < 0.05$ and $|\Delta d_{FS}| < 0.05$, indicating minimal structural change and proximity to a stationary point. (c) Scenario where $\Delta d_{IS} \cdot \Delta d_{FS} > 0$, showing the structure remains away from both IS and FS, often near a TS on a smooth PES. Red dashed curves denote regions where all points share the same optimization direction, while blue dashed arrows indicate the principal direction of structural evolution during optimization. The orange dots indicate the structures of the initial, transition, and final states, the blue dots represent the interpolated structures, and the red dots denote the structures obtained after conditional optimizing the blue dots.

Case 1: Minimal structural deviation

If both $|\Delta d_{IS}| < 0.05$ and $|\Delta d_{FS}| < 0.05$, the structure exhibits minimal geometric change during conditional optimization. This suggests that the initial interpolated structure is already close to a stationary point, such as a minimum or transition state, on the potential energy surface (PES), and the final optimized geometry has not deviated significantly from the starting point (Figure 3b).

Case 2: Nondirectional trajectory

If $|\Delta d_{IS}| \cdot |\Delta d_{FS}| > 0$, the structural optimization trajectory is nondirectional, i.e., the structure does not move closer to either IS or FS but remains in a region of the PES distant from both. This typically arises when the initial structure is located near the TS and the PES is relatively smooth along the reaction path, in which case a few optimization steps are sufficient to maintain proximity to the TS region. It should be noted that this criterion relies on the assumption of a locally smooth PES; for more complex systems with multiple nearby minima or substantial anharmonicities, its reliability may be reduced (see Figure 3c).

Above all, the D criteria provide a clear decision rule and are formally defined as follows:

$$D(R^{c-opt}) = \text{(a) } \Delta d_{IS} \cdot \Delta d_{FS} > 0 \text{ or (b) } |\Delta d_{IS}| < 0.05 \text{ and } |\Delta d_{FS}| < 0.05 \quad (7)$$

2.4 Step Details of RDA

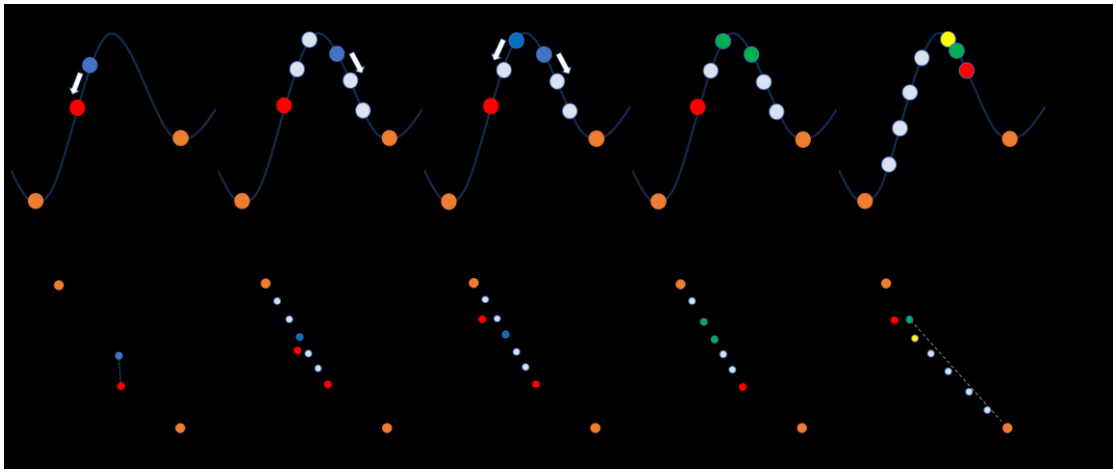

Figure 4. Demonstration of the RDA process for quasi-transition state (quasi-TS) identification. (a-e) One-dimensional case where the optimization direction of R_α points towards IS; interpolation is performed between R_α^{c-opt} and R_{FS}. (f-j) Two-dimensional case demonstration where the optimization direction of R_α points towards FS; interpolation is carried out between R_α^{c-opt} and R_{IS}. Panels (a-e) and (f-j) illustrate the same steps: (a) and (f) Pathway discretization and midpoint selection; (b)-(c) and (g)-(h) adaptive climbing and bracketing; (d) and (i) identification of R_{dc} (direction consistent) and R_{dnc} (direction non-consistent). (e) and (j) quasi-TS identification. The orange dots indicate the structures of the initial and final states, the blue dots represent the structures obtained through interpolation, and the red dots denote the interpolated structures after conditional optimization. Green dots highlight the two bracketing structures closest to the TS, which reside on opposite sides of the energy barrier as determined by optimization direction analysis. Finally, the yellow dots represent quasi-transition state. There, R_{dc} (direction consistent) refers to the structure closest to the TS that changes direction relative to R_α; R_{dnc} (direction none-consistent) refers to the structure closest to the TS that retains the same optimization direction as R_α.

2.4.1 Step 1: Conditional optimization for initial midpoint

The reaction pathway connecting the initial and final states (R_{IS} and R_{FS}) is discretized by linear interpolation. The interpolated structure R_α is generated as:

$$R_\alpha = (1-\alpha)R_{IS} + \alpha R_{FS} \quad (8)$$

where $\alpha = 0.5$. This R_α is then subjected to conditional optimization according to the convergence criteria described in Section 2.3.1. During conditional optimization, the evolution of R_α is monitored by calculating the Euclidean distances to both R_{IS} and R_{FS} at each step, providing insight into its relative position on the potential energy surface (PES) (see Figure 4a for optimization toward IS and Figure 4f for optimization towards FS).

Upon completion of the conditional optimization, the differences in Euclidean distances to IS and FS (Δd_{IS} and Δd_{FS}) are analyzed. The D criteria, as defined in Section 2.3.4, are applied to assess whether R_α is located near a stationary point on the PES. If the D criteria are satisfied, the dimer method is invoked directly. Otherwise, the workflow proceeds to step 2.

2.4.2 Step 2: Adaptive climbing and bracketing

In this step, a new round of linear interpolation is performed between R_{α}^{c-opt} and the reference structure (R_{ref}), typically chosen from among the R_{IS} or R_{FS}, as defined in Section 2.3.3. The interpolated structure R_{β} is generated as:

$$R_{\beta} = (1 - \beta)R_{\alpha}^{c-opt} + \beta R_{ref} \quad (9)$$

where β is initially set to 0.5. R_{β} is then subjected to conditional optimization, and the resulting directionality indices $\sigma(R_{\alpha}^{c-opt})$ and $\sigma(R_{\beta}^{c-opt})$ are evaluated (see Eq. 6).

If the optimization directions are inconsistent (i.e., $\sigma(R_{\alpha}^{c-opt}) \neq \sigma(R_{\beta}^{c-opt})$ (see Figure 4b), the transition state is bracketed between R_{α} and R_{β}, and the appropriate region for further exploration lies between these two structures. Accordingly, the interpolation coefficient β is decreased ($\beta \rightarrow \beta - \Delta\beta$) to generate new candidates closer to R_{α} and, thus, nearer to the TS region (Figure 4c). Conversely, if the optimization directions of R_{α} and R_{β} are consistent (i.e., $\sigma(R_{\alpha}^{c-opt}) = \sigma(R_{\beta}^{c-opt})$; see Figure 4g), this suggests the transition state is bracketed between R_{β} and R_{ref}, and the search region is shifted towards the reference structure. In this case, β is increased (e.g., $\beta \rightarrow \beta + \Delta\beta$), moving candidate structure closer to R_{ref}. Here, Δβ is defined as 0.1.

This adaptive iteration of β continues until a pair of structures is identified: one with the same optimization directionality as R_{α} (denoted as R_{dc}), while the other (R_{dnc}) with the opposite directionality (see Figure 4d and 4i). These two structures effectively bracket the transition state region on the potential energy surface. Once this bracketing condition is achieved, the workflow proceeds to step 3 for transition state refinement.

2.4.3 Step 3: Quasi-TS identification

After defining the two bracketing structures (R_{dnc} and R_{dc}), a new set of candidate structures is generated by performing a further linear interpolation between R_{dnc}^{c-opt} and R_{ref}:

$$R_{\gamma} = (1 - \gamma)R_{dnc}^{c-opt} + \gamma R_{ref} \quad (10)$$

where γ is initially set to 0.1. Starting from the candidate closest to R_{dnc} (γ = 0.1), structures are sequentially examined by comparing their Euclidean distance to R_{ref} with that of R_{dnc}. If the γ = 0.1 candidate still exhibits a larger distance, the next candidate is generated by increasing γ in increments of Δγ = 0.1. This procedure is repeated until the first candidate with a smaller distance than R_{dnc} is found, which is then designated as the quasi-TS. The rationale for choosing the first such candidate is that the convergence criterion in the preceding optimization (ΔE < 0.05) is relatively loose, resulting in fewer optimization steps. Thus, the candidate closest to R_{dnc} and geometrically nearer to the transition state is most likely to serve as the quasi-transition state (Figure 4e, 4j). Finally, the quasi-TS is then used as the initial guess for the dimer method, which rapidly converges to the precise TS.

3. RESULTS AND DISCUSSION

3.1 Computational details

In this work, density functional theory (DFT) calculations with Perdew-Burke-Ernzerhof (PBE)[38] functional were conducted using the Vienna Ab-initio Simulation Package (VASP)[39, 40]. The cut-off energy was set to 450 eV. A Monkhorst-Pack k-point 1×1×1 was used for structure optimization calculations of gas-phase reactions with a box of 20×20×20 Å, while 2×2×1 was applied for catalyzed reactions for unit cell of p(3×3). The structural optimization was based on the Residual Minimization Method with Direct Inversion (RMM-DIIS). The force convergence was set to be 0.05 $eV \cdot Å^{-1}$ for either structure optimizations or dimer. For comparison, the NEB method was also performed to locate the TS of the same reactions and images were interpolated between the initial state and the final state using the linear interpolation method. In the study of catalysed reactions, a vacuum space of more than 10 Å was placed above the slabs to avoid interactions between the periodic images. In the process of structure optimization, all atoms of the reactants and the top two layers of the slab were allowed to relax freely, while the bottom two layers of the slab were fixed.

3.2 Applications in Gas-phase Reactions

To evaluate the efficiency of the RDA-D method, 24 gas-phase reactions were selected from Baker's benchmark dataset.[35] The evaluation results on computational cost and efficiency of TS searches using the RDA-D and NEB methods are summarized in Table 1.

Table 1. Comparison of the RDA-D method and the NEB for finding TSs in gas-phase reactions.

no.	reaction	atoms	NEB/RDA-D	
			cpu	gradient
1	HCN ↔ HNC	3	2.51	1.15
2	HCCH ↔ CCH_2	4	22.19	12.18
3	H_2CO ↔ H_2 + CO	4	1.28	1.73
4	CH_3O ↔ CH_2OH	5	2.66	1.37
5	cyclopropyl ring opening	8	1.29	1.31
6	bicyclo[1,1,0] butane TS1	10	3.02	2.40
7	1,2-migration-(formyloxy)ethyl	10	5.71	2.32
8	parent Diels-Alders	16	42.10	24.33
9	s-tertrazine ↔ 2HCN + N_2	8	6.54	5.31
10	trans-butadiene ↔ cis-butadiene	10	1.42	1.48
11	CH_3CH_3 ↔ CH_2CH_2 + H_2	8	2.68	1.51

12	$CH_3CH_2F \leftrightarrow CH_2CH_2 + HF$	8	1.84	1.70
13	vinyl alcohol ↔ acetaldehyde	7	4.55	3.19
14	$HCOCl \leftrightarrow HCl + CO$	4	3.46	2.34
15	$H_2PO_4^+ \leftrightarrow H_2O + PO_3^+$	7	9.60	8.50
16	Claisen rearrangement	14	12.42	5.24
17	$SiH_3CH_2CH_3 \leftrightarrow SiH_2 + CH_3CH_3$	11	1.18	1.14
18	$HNCCS \leftrightarrow HNC + CS$	5	7.41	3.50
19	$HCONH_3^+ \leftrightarrow NH_4^+ + CO$	7	4.38	2.88
20	rotational TS in acrolein	8	1.59	2.17
21	OCHNHOH ↔ HOCHNOH	7	2.03	2.86
22	$H_2CNH \leftrightarrow HNC + H_2$	5	7.29	6.59
23	$H_2CNH \leftrightarrow HCNH_2$	5	2.29	2.46
24	$HCNH_2 \leftrightarrow HCN + H_2$	5	4.73	4.41
ave			6.42	4.25

The table compares the computational cost and the number of structural optimization steps required by the NEB and RDA-D methods in locating transition states (TS) for 24 gas-phase reactions from Baker's benchmark dataset. The reactions encompass a variety of mechanisms, including isomerization, dissociation, insertion, rearrangement, ring-opening, and ring-formation, with the number of atoms in the systems ranging from 3 to 16. Across the dataset, RDA-D consistently outperforms NEB in computational efficiency. On average, RDA-D is approximately 6.42 times faster than NEB in terms of CPU time and requires about 4.25 times fewer gradient calculations. For simpler systems, for example Reactions 1 and 5, RDA-D performs comparably to NEB, albeit with reduced computational costs and fewer optimization steps. However, for complex reactions, such as Reaction 8 (a ring-formation reaction), RDA-D yields substantial improvements over NEB, with markedly fewer optimization steps and reduced CPU time. These results highlight the robustness and superior computational efficiency of RDA-D for transition-state searches in gas-phase reactions.

3.3 Applications in Heterogeneous Catalysis Reactions

To assess the effectiveness of the RDA-D method for heterogeneous catalysis reactions, we selected 8 reactions as a test set.[41-53] These 8 reactions encompass two major categories: different reactions on the same surface and the same reaction on different surfaces. Furthermore, the reactions include three fundamental reaction types as described in our previous work:[46] dehydrogenation (Class I); diatomic molecule activation and hydrocarbon cracking (Class II); and triatomic activation (Class III). The computational cost and efficiency of TS searches using the RDA-D and NEB methods are summarized in Table 2.

Table 2. Comparison of the RDA method and the NEB for finding TSs in heterogeneous catalysis. Five typical reactions on different catalysts are compared using our method and NEB.

surface	reaction	atoms	NEB/RDA-D		class
			cpu	gradient	
Pt(111)	$CO + O \leftrightarrow CO_2$	39	3.86	5.69	III
Pt(111)	C+ H ↔ CH	38	3.09	3.10	I
Pt(111)	C + O ↔ CO	38	1.62	2.20	II
Pt(111)	C + N ↔ CN	38	13.53	23.33	II
Pt(111)	$N + N \leftrightarrow N_2$	38	3.46	2.87	II
Pt(211)	C+ H ↔ CH	26	3.68	5.47	I
Pt(211)	C + O ↔ CO	26	5.14	3.46	II
Pt(211)	C + N ↔ CN	26	2.77	2.32	II
ave			4.64	6.05	

The table summarizes the performance of the NEB and RDA-D methods in locating transition states (TS) for a set of 8 surface reactions occurring on Pt(111) and Pt(211). These reactions involve systems ranging from 26 to 39 atoms and span multiple reaction classes. On average, RDA-D is approximately 4.64 times faster than NEB in terms of CPU time and requires about 6.05 times fewer gradient evaluations, demonstrating both the stability and computational efficiency of the method.

The geometries of ISs, TSs, and FSs of the selected reactions are shown in Figure 5. Taking the TS searching process on Pt(111) using the $CO + O \leftrightarrow CO_2$ reaction as an example (as shown in Figure 5k), the RDA-D workflow proceeds as follows:

(i) The workflow begins with the initial and final states (IS and FS). The interpolated midpoint R_α is generated and then subjected to conditional optimized for several steps, yielding R_α^{c-opt}. The optimization direction of R_α^{c-opt} point towards IS. Application of the D criteria indicates that it is not sufficiently close to a stationary point.

(ii) A new midpoint R_β ($\beta = 0.5$) is generated by interpolation between R_α^{c-opt} and the R_{FS}, which is subsequently selected for conditional optimization. The conditional optimized structure R_β^{c-opt} still points towards IS. To induce a change in optimization direction, the weight of the FS in the interpolation is incrementally increased ($\beta \rightarrow \beta + 0.1$), and $R_{\beta+0.1}$ is optimized and reassessed. This process is repeated until $R_{\beta+0.2}^{c-opt}$ is obtained, which points the FS, indicating a direction reversal. At this stage, $R_{\beta+0.2}$ and $R_{\beta+0.1}$ are identified as R_{dnc} (direction non-consistent) and R_{dc} (direction consistent), respectively.

(iii) The further interpolation is performed between the R_{dnc}^{c-opt} and R_{IS}. Among the

generated candidates, the first structure closer to R_{ref} than R_{dnc} is designated as the quasi-TS. quasi-TS. Finally, the quasi-TS is refined to precisely locate the TS, completing the workflow.

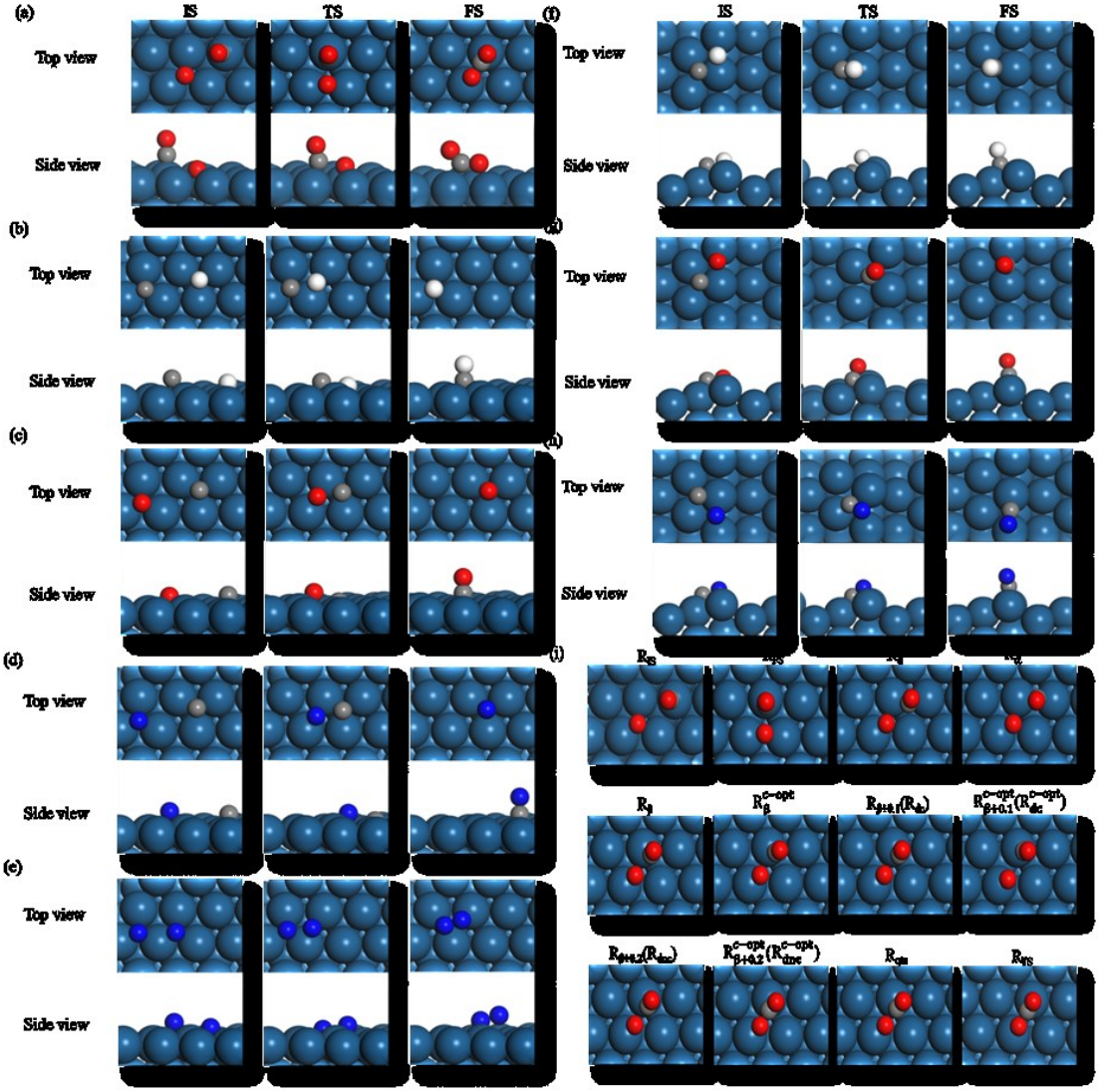

Figure 5. Top and side view representations of IS, TS, and FS structures on Pt(111) for the following reactions: (a) CO + O ↔ CO_2, (b) C+ H ↔ CH, (c) C + O ↔ CO, (d) C + N ↔ CN, (e) N + N ↔ N_2. Top and side view representations of IS, TS, and FS structures on Pt(211) for the following reactions: (f) C+ H ↔ CH, (g) C + O ↔ CO, (h) C + N ↔ CN. (i) TS searching process for the CO + O ↔ CO_2 reaction on Pt(111) as a representative example. The stepwise interpolation and conditional optimization enable identification of the quasi-TS, which is subsequently refined using the dimer method to precisely locate the precise TS.

Both methods utilize identical initial and final structures as starting points; however, NEB requires a larger number of images to fully describe the reaction pathway, which in turn leads to more gradient evaluations per iteration. For complex reactions with highly convoluted pathways, NEB can therefore become computationally expensive and prone to convergence difficulties. In contrast, RDA-D significantly reduces the

computational burden by adaptively focusing on critical regions of the potential energy surface (PES). Typically, the RDA method achieves quasi-TS identification in no more than three rounds of interpolation, with as few as one and no more than six structures conditionally optimized, even in challenging cases. By integrating the dimer method for refinement, RDA-D not only eliminates the need for an initial guess required by the dimer approach but also preserves high accuracy and efficiency. Importantly, RDA-D successfully located all TSs for both gas-phase and surface reactions in the test set, demonstrating the robustness and versatility of the RDA-D based approach for TS searches.

4. CONCLUSIONS

In this work, we presented the Reaction Directional Analysis with Dimer refinement (RDA-D) method as a systematic and efficient approach for transition state (TS) searching across a wide range of reactions. By combining dynamic interpolation, structural optimization, directional analysis, and structure screening, RDA offers a robust and automated framework for quasi-TS identification. The method efficiently narrows the search space, quantitatively evaluates candidate structures, and guides conditional optimization towards the TS region.

A key advantage of RDA-D is its independence from predefined reaction coordinates or chemical intuition, requiring only the initial and final states as input, which makes it highly versatile and user-friendly. Furthermore, by incorporating the dimer method for further refinement, RDA-D overcomes the challenge of providing an initial guess for dimer-based approaches, while maintaining both high accuracy and efficiency.

Compared to traditional methods such as the Nudged Elastic Band (NEB), which rely on multiple intermediate images, RDA-D dynamically refines candidate structures and focuses computational effort on critical regions of the potential energy surface (PES). Benchmark tests on diverse gas-phase and catalytic reactions on solid surfaces demonstrate that RDA-D is, on average, 5.70 times faster than NEB in terms of CPU time, and reduces the number of gradient calculations by a factor of 4.67, while maintaining energy accuracy.

The automation-friendly design and scalability of RDA-D make it a promising tool for automated exploration of complex PES landscapes, catalyst screening, and mechanistic studies in heterogeneous systems. Its ability to handle diverse reaction types with minimal user intervention establishes RDA-D as a powerful and versatile method for TS searching, offering both computational efficiency and robustness for fundamental and applied research in chemistry.

ASSOCIATED CONTENT

Supporting Information.

Cartesian coordinates of all optimized structures are provided in the Supporting Information (PDF).

AUTHOR INFORMATION

Corresponding Author
*** Email for C.X.G:** guochenxi@supcon.com
*** Email for P.H.:** hupj@shanghaitech.edu.cn

Author Contributions

P.H and C.X.G conceived the project. P.P.Z carried out all the calculations. P.P.Z wrote the first draft of the manuscript and prepared figures and all the authors contributed to the revision of the manuscript.

Notes

The authors declare no competing financial interest.

ACKNOWLEDGEMENTS

NKRDPC (2021YFA1500700) and NSFC (92045303) are acknowledged.

REFERENCES

1. Liu, Y.; Qi, H.; Lei, M. Improved elastic image pair method for finding transition states. *J. Chem. Theory Comput.* **2023,** *19*, 2410-2417.
2. Liu, Z.-P. Chemical reactions at surfaces and interfaces from first principles: Theory and application. *Pure Appl. Chem.* **2004,** *76*, 2069-2083.
3. Schlegel, H. B. Exploring potential energy surfaces for chemical reactions: an overview of some practical methods. *J. Comput. Chem.* **2003,** *24*, 1514-1527.
4. Lewis-Atwell, T.; Townsend, P. A.; Grayson, M. N. Machine learning activation energies of chemical reactions. *Wiley Interdiscip. Rev. Comput. Mol. Sci.* **2022,** *12*, e1593.
5. Park, S.; Han, H.; Kim, H.; Choi, S. Machine learning applications for chemical reactions. *Chem. Asian J.* **2022,** *17*, e202200203.
6. Ismail, I.; Robertson, C.; Habershon, S. Successes and challenges in using machine-learned activation energies in kinetic simulations. *J. Chem. Phys.* **2022,** *157*, 014801.
7. Henkelman, G.; Uberuaga, B. P.; Jónsson, H. A climbing image nudged elastic band method for finding saddle points and minimum energy paths. *J. Chem. Phys.* **2000,** *113*, 9901-9904.
8. Jonsson, H.; Mills, G.; Jacobsen, K. W. *Nudged Elastic Band Method for Finding Minimum Energy Paths of Transitions;* World Scientific: Singapore, **1998,** pp 385-404.
9. Zhao, L.; Watanabe, K.-j.; Nakatani, N.; Nakayama, A.; Xu, X.; Hasegawa, J.-y. Extending nudged elastic band method to reaction pathways involving multiple spin states. *J. Chem. Phys.* **2020,** *153*, 134115.
10. Galván, I. F.; Field, M. J. Improving the efficiency of the NEB reaction path finding algorithm. *J. Comput. Chem.* **2008,** *29*, 139-143.

11. Weinan, E.; Ren, W.; Vanden-Eijnden, E. String method for the study of rare events. *Physical Review B* **2002,** *66*, 052301.
12. Ren, W.; Vanden-Eijnden, E. Simplified and improved string method for computing the minimum energy paths in barrier-crossing events. *J. Chem. Phys.* **2007,** *126,* 164103.
13. Behn, A.; Zimmerman, P. M.; Bell, A. T.; Head-Gordon, M. Efficient exploration of reaction paths via a freezing string method. *J. Chem. Phys.* **2011,** *135*, 224108.
14. Suleimanov, Y. V.; Green, W. H. Automated discovery of elementary chemical reaction steps using freezing string and Berny optimization methods. *J. Chem. Theory Comput.* **2015,** *11*, 4248-4259.
15. Zhang, X.-J.; Shang, C.; Liu, Z.-P. Double-ended surface walking method for pathway building and transition state location of complex reactions. *J. Chem. Theory Comput.* **2013,** *9*, 5745-5753.
16. Zhang, J.; Chen, J.; Hu, P.; Wang, H. Identifying the composition and atomic distribution of Pt-Au bimetallic nanoparticle with machine learning and genetic algorithm. *Chin. Chem. Lett.* **2020,** *31*, 890-896.
17. Zhang, J.; Hu, P.; Wang, H. Amorphous catalysis: machine learning driven high-throughput screening of superior active site for hydrogen evolution reaction. *J. Phys. Chem. C.* **2020,** *124*, 10483-10494.
18. Mauro, J. C.; Loucks, R. J.; Balakrishnan, J. A simplified eigenvector-following technique for locating transition points in an energy landscape. *J. Phys. Chem. A*. **2005,** *109*, 9578-9583.
19. Ásgeirsson, V.; Birgisson, B. O.; Bjornsson, R.; Becker, U.; Neese, F.; Riplinger, C.; Jónsson, H. Nudged elastic band method for molecular reactions using energy-weighted springs combined with eigenvector following. *J. Chem. Theory Comput.* **2021,** *17*, 4929-4945.
20. Henkelman, G.; Jónsson, H. A dimer method for finding saddle points on high dimensional potential surfaces using only first derivatives. *J. Chem. Phys.* **1999,** *111*, 7010-7022.
21. Chen, P.; Liu, Y.; Xu, Y.; Guo, C.; Hu, P. Quantitative Evidence to Challenge the Traditional Model in Heterogeneous Catalysis: Kinetic Modeling for Ethane Dehydrogenation over Fe/SAPO-34. *JACS Au.* **2022,** *3*, 165-175.
22. Guo, C.; Mao, Y.; Yao, Z.; Chen, J.; Hu, P. Examination of the key issues in microkinetics: CO oxidation on Rh(111). *J. Catal.* **2019,** *379*, 52-59.
23. Fu, X.; Li, J.; Long, J.; Guo, C.; Xiao, J. Understanding the product selectivity of syngas conversion on ZnO surfaces with complex reaction network and structural evolution. *ACS Catal.* **2021,** *11*, 12264-12273.
24. Guo, C.; Fu, X.; Long, J.; Li, H.; Qin, G.; Cao, A.; Jing, H.; Xiao, J. Toward computational design of chemical reactions with reaction phase diagram. *Wiley Interdiscip. Rev. Comput. Mol. Sci.* **2021,** *11*, e1514.
25. Wang, H.-F.; Liu, Z.-P. Comprehensive mechanism and structure-sensitivity of ethanol oxidation on platinum: new transition-state searching method for resolving the complex reaction network. *J.Am.Chem.Soc.* **2008,** *130*, 10996-11004.
26. Shang, C.; Liu, Z.-P. Constrained Broyden Minimization Combined with the Dimer

Method for Locating Transition State of Complex Reactions. *J. Chem. Theory Comput.* **2010,** *6*, 1136-1144.
27. Shang, C.; Liu, Z.-P. Constrained Broyden Dimer Method with Bias Potential for Exploring Potential Energy Surface of Multistep Reaction Process. *J. Chem. Theory Comput.* **2012,** *8*, 2215-2222.
28. Shang, C.; Liu, Z.-P. Stochastic Surface Walking Method for Structure Prediction and Pathway Searching. *J. Chem. Theory Comput.* **2013,** *9*, 1838-1845.
29. Khait, Y. G.; Puzanov, Y. V. Search for stationary points on multidimensional surfaces. *J. Mol. Struct.: THEOCHEM.* **1997**, 398-399, 101-109.
30. Banerjee, A.; Adams, N.; Simons, J.; Shepard, R. Search for stationary points on surfaces. *J. Chem. Phys.* **1985,** *89*, 52-57.
31. Baker, J. An algorithm for the location of transition states. *J. Comput. Chem.* **1986,** *7*, 385-395.
32. Peters, B.; Heyden, A.; Bell, A. T.; Chakraborty, A. A growing string method for determining transition states: Comparison to the nudged elastic band and string methods. *J. Chem. Phys.* **2004,** *120*, 7877-7886.
33. Zimmerman, P. Reliable transition state searches integrated with the growing string method. *J. Chem. Theory Comput.* **2013,** *9*, 3043-3050.
34. Sun, Y. Efficient acceleration of the convergence of the minimum free energy path via a path-planning generated initial guess. *J. Comput. Chem.* **2025,** *46*, e27504.
35. Baker, J.; Chan, F. The location of transition states: A comparison of Cartesian, Z-matrix, and natural internal coordinates. *J. Comput. Chem.* **1996,** *17*, 888-904.
36. Halgren, T. A.; Lipscomb, W. N. The synchronous-transit method for determining reaction pathways and locating molecular transition states. *Chem. Phys. Lett.* **1977,** 49, 225-232.
37. Smidstrup, S.; Pedersen, A.; Stokbro, K.; Jónsson, H. Improved initial guess for minimum energy path calculations. *J. Chem. Phys.* **2014**, 140, 214106.
38. Perdew, J. P.; Burke, K.; Ernzerhof, M. Generalized gradient approximation made simple. *Phys. Rev. Lett.* **1996,** *77*, 3865.
39. Kresse, G.; Furthmüller, J. Efficiency of ab-initio total energy calculations for metals and semiconductors using a plane-wave basis set. *Comput. Mater. Sci.* **1996,** *6*, 15-50.
40. Kresse, G.; Hafner, J. Ab initio molecular-dynamics simulation of the liquid-metal-amorphous-semiconductor transition in germanium. *Phys. Rev. B: Condens. Matter.* **1994,** *49*, 14251-14269.
41. Scaranto, J.; Mavrikakis, M. HCOOH decomposition on Pt(111): A DFT study. *Surf. Sci.* **2016,** *648*, 201-211.
42. Offermans, W.; Jansen, A.; Van Santen, R.; Novell-Leruth, G.; Ricart, J.; Perez-Ramirez, J. Ammonia dissociation on Pt(100), Pt(111), and Pt(211): a comparative density functional theory study. *J. Phys. Chem. C* **2007,** *111*, 17551-17557.
43. Alavi, A.; Hu, P.; Deutsch, T.; Silvestrelli, P. L.; Hutter, J. CO oxidation on Pt(111): an ab initio density functional theory study. *Phys. Rev. Lett.* **1998,** *80*, 3650.
44. Liu, Z.-P.; Hu, P. General trends in CO dissociation on transition metal surfaces. *The J. Chem. Phys.* **2001,** *114*, 8244-8247.

45. Mukerji, R. J.; Bolina, A. S.; Brown, W. A.; Liu, Z.-P.; Hu, P. The temperature dependence of the adsorption of NO on Pt(211): a RAIRS and DFT investigation. *J. Phys. Chem. B* **2004,** *108*, 289-296.
46. Michaelides, A.; Liu, Z.-P.; Zhang, C.; Alavi, A.; King, D. A.; Hu, P. Identification of general linear relationships between activation energies and enthalpy changes for dissociation reactions at surfaces. *J.Am.Chem.Soc.* **2003,** *125*, 3704-3705.
47. Chen, Y.; Vlachos, D. G. Density functional theory study of methane oxidation and reforming on Pt(111) and Pt(211). *Ind. Eng. Chem. Res.* **2012,** *51*, 12244-12252.
48. Ford, D. C.; Nilekar, A. U.; Xu, Y.; Mavrikakis, M. Partial and complete reduction of O_2 by hydrogen on transition metal surfaces. *Surf. Sci.* **2010,** *604*, 1565-1575.
49. Michaelides, A.; Hu, P. The valency effect on reaction pathways in heterogeneous catalysis: insight from density functional theory calculations. In *Theoretical Aspects of Heterogeneous Catalysis*; Joyner, R. W.; van Santen, R. A., Eds.; Springer: Dordrecht, **2001**; pp 199-215.
50. Michaelides, A.; Hu, P. Softened C-H modes of adsorbed methyl and their implications for dehydrogenation: An ab initio study. *J. Chem. Phys.* **2001,** *114*, 2523-2526.
51. Michaelides, A.; Hu, P. Catalytic water formation on platinum: A first-principles study. *J.Am.Chem.Soc.* **2001,** *123*, 4235-4242.
52. Liu, Z.-P.; Hu, P.; Alavi, A. Mechanism for the high reactivity of CO oxidation on a ruthenium-oxide. *J. Chem. Phys.* **2001,** *114*, 5956-5957.
53. Liu, Z.-P.; Hu, P. General rules for predicting where a catalytic reaction should occur on metal surfaces: a density functional theory study of C-H and C-O bond breaking/making on flat, stepped, and kinked metal surfaces. *J.Am.Chem.Soc.* **2003,** *125*, 1958-1967.